Chapter 7
Optoelectronics

Jaroslav Kováč , František Uherek, Daniel Donoval, Jaroslav Kováč jr., and Alexander Šatka

Abstract Optoelectronics covers the design, manufacture, and characterization of hardware devices that convert electrical signals into photon signals and vice-versa. The interaction between light and matter lies at the heart of optoelectronics, and progress in this area impacts all fields of application, including light sources, detectors, and optical communication systems. A brief review of the performance and development of up-to-date light-emitting diodes (LEDs) and photodetectors applicable in information technology is presented. After a short introduction into the physics and technology of semiconductor optoelectronic devices, their potential importance for future optoelectronics and photonics applications are discussed. Examples, where III–V compound semiconductors are used in LEDs, resonant cavity enhanced and avalanche photodetector structures, as well as new materials and structures for efficient visible light emitting diodes based on organic semiconductors are discussed. Key problems that are still to be addressed with regard to the need for interdisciplinary integration consistent with More than Moore domain in ENIAC strategy research agenda are also identified.

Keywords III–V semiconductors • Organic semiconductors • Optoelectronic devices • LEDs • OLEDs • Photodetectors • RCE p-i-n • APD • Optical communication systems • Silicon photonics

7.1 Introduction

If you use electric lights, remote-controlled televisions, compact disc players, computers, or the fiber optic networks, which link modern telephones, optoelectronics has become integral part of today's life. The concept of using optical processes to

---

J. Kováč (✉), F. Uherek, D. Donoval, J. Kováč jr., and A. Šatka
Faculty of Electrical Engineering and Information Technology STU,
Ilkovičova 3, 81219 Bratislava, Slovakia
e-mail: jaroslav.kovac@stuba.sk

G.Q. Zhang and A.J. van Roosmalen (eds.), *More than Moore: Creating High Value Micro/Nanoelectronics Systems*,
DOI 10.1007/978-0-387-75593-9_7, © Springer Science+Business Media, LLC 2009

perform useful functions is known as optoelectronics, electro-optics, or photonics, and it is a new area for future. Photonics harnessing the potential of light across a broad spectrum of applications including communications and information processing and optoelectronics is the alliance of optics and electronics. Optoelectronics covers the design and manufacture of hardware devices that convert electrical signals into photon signals and vice-versa. In the large frequency band from infrared to ultraviolet, it deals with problems of light generation, detection, transmission, technology of advanced materials needed to manufacture optoelectronic components, and their utilizations not only in various technologies including fiber optic communications, laser systems, cameras, remote sensing systems, data storage, and optical information systems but also with systems for medicine, environment protection, industrial and military applications. Photonics has been identified as a key technology with far reaching influences in communications, transportation, medicine, manufacturing, construction, computing, and defense. It is generally expected that optoelectronics and light (photons) will replace electrons as the principal information carrier in the near future [1].

Optoelectronics as applied to telecommunications, data communications, CATV, data storage displays and imaging is characterized by a prodigious global growth and spectacular technological innovations. Two main driving forces lie behind the development of the optoelectronic devices and integrated optoelectronic components and structures. First, our information age brings a daily increasing demand on data transfer, storage, and imaging. This pushes forward – among others – optical communication technologies that are capable of transmitting huge amounts of information over distances ranging from millimeters to thousands of kilometers. A concept for increasing transfer rates of the existing and future optical links is the wavelength division multiplex (WDM), where data are transmitted by light of different wavelengths simultaneously via the same optical fiber [2]. Besides this motivation, the second driving force for the development of the entire range of modern optoelectronic devices is the rapid development of modern semiconductor technologies. This allows continuous research and development of lasers, detectors and fiber-optical components, powerful transmitter and receiver modules for medium and long-range communication. Additionally, the development of new materials and structures for efficient visible light-emitting diodes (LEDs) based on wide band gap III-nitride semiconductors and organic semiconductors such as organic light-emitting diodes (OLEDs) is of growing interest.

Novel approaches are explored daily to improve the current optoelectronics state of-the-art. Such improvements will extend the usage and the efficiency of new light sources including solid-state-lighting, support the rising information technology age for displays and high density optical data storage, and enhance the environmental awareness capabilities of humans by utilization of ultraviolet and visible photon detectors and sensors [3].

In addition, a new field of nanotechnology enables all components of a transmitter or receiver to be integrated on a single chip and very likely this integration process will lead to increased performance and reduced production costs, as was the case in integrated micro and optoelectronics.

The application of nanotechnology in optoelectronics is not limited to active devices. Modern epitaxial techniques such as MBE and metalorganic chemical vapour deposition (MO CVD) allow the growth of precisely defined thin semiconductor layers with perfectly flat interfaces. They provide technological basis for novel optoelectronic devices with enhanced optical properties. The application of quantum wells (QWs) instead of bulk materials as an active layer of LEDs, photodetectors, and semiconductor lasers have significantly improved their performance in both static and dynamic modes of operation. A further improvement of semiconductor devices performance is expected with the introduction of multidimensional quantum confinement to wire-like quantum wires (QWr) and box-like quantum dots (QD) of sufficient small lateral dimensions less than a few nanometers [4]. In particular, microcavity devices such as vertical cavity surface emitting lasers (VCSELs), resonant cavity enhanced (RCE) LEDs, photodetectors, and modulators have recently received increased interest in optical interconnect technology [5]. They benefit from enclosing a conventional semiconductor structure into an optical resonant cavity grown usually in the same epitaxial process as the device itself.

Recently, development of new materials and structures for efficient visible LEDs is of growing interest. The world at the end of the twentieth century has witnessed a blue rush toward the development of violet-blue-green LEDs and laser diodes (LDs) based on GaN wide band gap III-nitride semiconductors [6]. First, the hard work has culminated with the demonstration of commercial high brightness blue and green LEDs and of commercial violet LDs.

New types of LEDs, lasers, detectors, and other photonic devices will become possible by the use of inorganic and recently of new organic semiconductors. Organic LEDs and organic FETs have underwent dramatic improvements in performance in the last 5 years [7]. The existing achievements in device area have greatly stimulated the studies in the related aspects of research in semiconductor organic materials. A bright future is forecasted for organic LEDs. Various applications ranging from organic displays, organic solid-state-lighting, to integrated sensor systems are expected to produce a huge impact on our future daily life.

7.2 Optoelectronics Devices

7.2.1 III–V semiconductor Materials for Optoelectronic Devices

One of the most important aspects of III-V compound semiconductors is the availability of bulk crystalline substrates of GaAs and InP, which can be obtained from commercial sources. The most commonly used III–V compounds are shown in Fig. 7.1, which plots their band gap as a function of the lattice constant, where the solid and dash lines represent direct and indirect band gaps, respectively.

An important aspect of a direct band gap semiconductor is that the minimum energy in the conduction band Brillouin zone occurs at the same k value as the

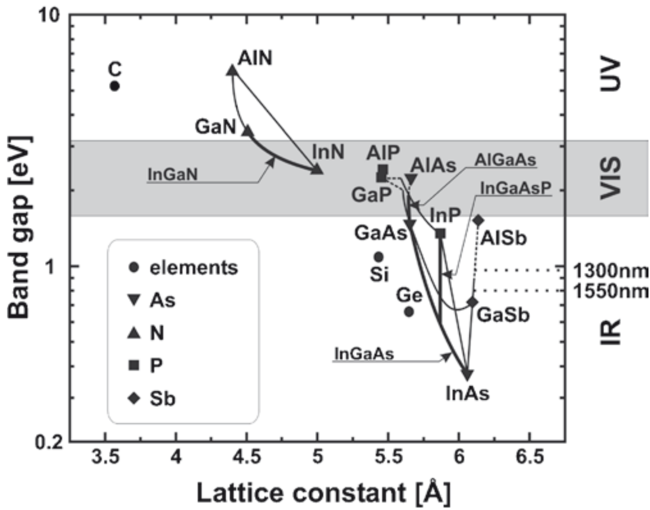

Fig. 7.1 Plot of the energy gap vs. lattice constant to some important semiconductors. *Lines* connecting points on the graph show the band gap and lattice constant variation

maximum energy of the valence band. This means that electrons can make transitions between the two bands without having to lose or gain momentum in the process. Therefore, in direct band gap semiconductor, the electron-hole pairs can recombine directly and emit photons. The majority of light emitting devices use direct band gap semiconductors such as GaAs, InP, GaN. In the case of indirect band gap semiconductor, such as Si or GaP, the minimum energy in the conduction band is not directly above the maximum energy of valence band but it is displaced on the *k* axis [8]. Any necessary loss or gain of the momentum always involves a third entity, a phonon for example, and this makes the transition much less probable. Hence, a direct band gap material is much more efficient for light sources than an indirect band gap material [9]. Different ranges of band gap energy can be obtained by mixtures of binary compounds. For example, the ternary compound $Al_xGa_{1-x}As$ can be made to have a band gap between 1.4 and 2.2 eV. By varying the ratio of Al to Ga, it becomes an indirect gap at a high Al content. The most important semiconductors for optical communications are mixed crystals based on GaAs and InP [8]. The quaternary $In_{1-x}Ga_xAs_yP_{1-y}$ can be grown on InP by lattice matching and its band gap can be tuned over the range 1.35–0.75 eV (0.95–1.67 μm), as shown in Fig. 7.1. Thus band gap engineering will generally choose the substrate, and then a suitable alloy, which has the required band gap. Band gap engineering is now a sophisticated and extremely valuable technology providing materials for optoelectronic devices.

Binary, ternary, and quaternary III–V alloy layers can be grown mostly using the epitaxial deposition techniques, such as molecular beam epitaxy (MBE) and MO CVD. In the MBE technique, the substrate is exposed to a thermal beam of

atoms and molecules that compose the semiconductor in ultrahigh vacuum typically 5×10^{-11} mbar or better. The advantages of MBE grown structures include highly abrupt junctions between different materials, good control over the thickness of layers at about 1 monolayer per second, and reasonable reproducibility [10]. In the MOCVD technique, the heated substrates are exposed to a hot stream of gaseous compounds. The composition of the gases can be varied rapidly to control the composition of the material grown. MOCVD has a reputation of producing better optoelectronic devices than MBE. It is also faster and has been successfully used for commercial production, growing on a large number of wafers simultaneously [11].

7.2.2 *Quantum Confined Effect in Low-Dimensional Semiconductor Structures*

In the last decades, much effort has been devoted to the study of two-dimensional (2D) semiconductor QWs. Most of the effort has concerned with understanding the basic quantum mechanical effects in QWs and their potential applications for optoelectronic devices [12]. If a semiconductor with a smaller band gap (GaAs) is sandwiched between layers of a larger band gap semiconductor (AlGaAs), and if the thickness of the smaller band material is comparable to or smaller than the carrier de Broglie wavelength in the semiconductor, the quantum confined effects in QW become important and lead to a profound change in the properties of semiconductors. The changes result from the fact that carriers are confined along the growth direction z but are free in x and y directions. The confinement of the carriers leads to quantitization of the eigenenergies in the direction of restriction and to a parabolic dispersion due to the motion in all remaining directions. The energies and dispersion of such subbands in a 2D system are illustrated in Fig. 7.2 for the case of a GaAs/AlGaAs quantum well. The subband energies are shifted with respect to the bulk band gap by the confinement energies $E_{n_z,q}$ $(q = e,h)$ of electrons and holes, which are given for an infinite-height of the quantum well with width L_z by $E_{n_z,q} = \hbar^2 n_z^2 \pi^2 / 2m_q L_z^2$, where n_z is the quantum number and m_q is the electron or hole effective mass.

Because of the smaller effective mass of electrons, quantization in the conduction band is much more pronounced than in the valence band. The first light hole (lh) level lies typically farther from the valence band edge than the respective heavy hole (hh) level because of the lighter effective mass. If multiple QWs are stacked on top of each other, either a multiquantum well (MQW) or a superlattice (SL) structure is formed. The difference between these two types is that in the superlattice, the QWs are so close to each other such that the electron wavefunction is not localized into a single QW. The density of states distribution in QW is no longer a smooth parabolic curve as for the bulk semiconductor (3D) but it has a staircase structure shown in Fig. 7.3. More recently, great interest has been raising in even lower-dimensional heterostructures such as one-dimensional (1D) quantum wires

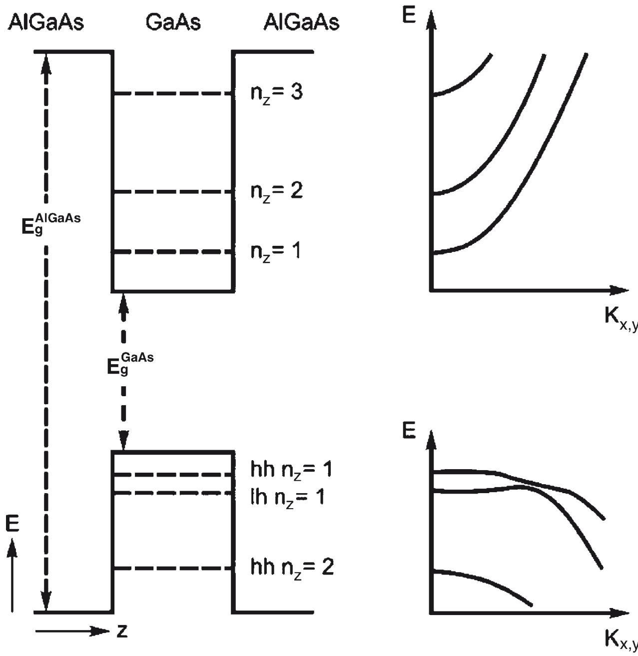

Fig. 7.2 Confined electron and hole energy levels and subband dispersion in AlGaAs/GaAs QW

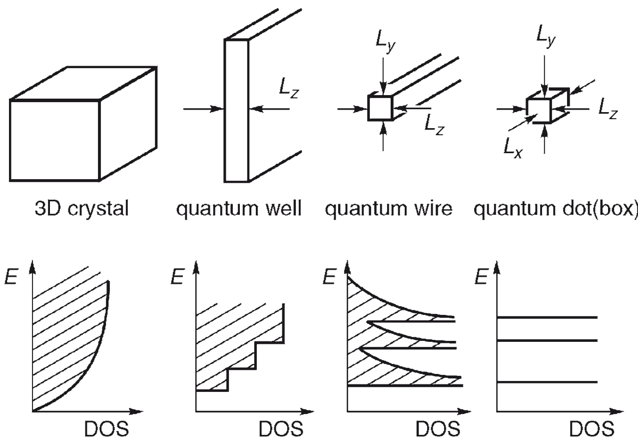

Fig. 7.3 Shape and density of states (DOS) in low dimensional (2D, 1D, 0D) semiconductor structures

(QWr) and zero-dimensional (0D) QD. However, the lack of technological capability in the fabrication of high-quality 1D and 0D heterostructures has so far limited the number of their possible applications. The electronic states in 1D and 0D structures

are described in a similar way. The additional lateral confinement of the wave functions, along the y axis in QWR and along x and y axes in QD, results in a larger confinement energy for the discrete electronics states. The carrier confinement strongly modifies the properties of excitons (bound electron-hole pairs) in these low-dimensional structures with respect to the bulk.

During the last few years, there has been an intense theoretical interest in physics of 1D electron systems quantum wires, which are predicted to exhibit unique electronic and optical properties [13, 14].

Intensive investigations in QD structures have been motivated by promising QD properties such as δ-function-like density of states (Fig. 7.3) and by the perspective of realizing QD devices such as low-threshold QD lasers. QDs are typically 2–10 nm in diameter. Because of extremely small size of QDs, their optical and electrical properties are largely determined by quantum mechanics rather than by classical physics. The material can be made from just about any known semiconductor, and QD have been synthesized from silicon, germanium, gallium arsenide, indium phosphide, cadmium selenide, and zinc sulfide to name a few [15]. QDs are being analyzed for uses as LEDs, lasers, flat screen displays, memory, and solar sensors.

7.2.3 LEDs and OLEDs Basic Concept

LEDs are typical p–n junction devices used under a forward bias that emit incoherent light, when current passes through the semiconductor junction. The important property of a p–n junction is the current-voltage characteristic. The current under forward bias is given by $I = I_0 \exp[(eU / k_b T) - 1]$, where I_0 is the saturation current, U is the applied forward voltage, e is the electron charge, k_b is Boltzmann's constant, and T is the absolute temperature. When current passes through the junction, the injected minority charge carriers recombine radiatively with the majority charge carriers emitting photons within the active region. This is the basic light generation process in semiconductors. The wavelength of the light emitted λ_g [μm] is approximately determined by the band gap energy E_g [eV] given by $\lambda_g = 1.24/E_g$. Depending on the semiconductor material used in the active layer, the wavelength of the emitted light can be anywhere within the range from UV to infrared.

In general, LEDs can be realized on both homojunction and heterojunction structures. The homojunction LEDs have two drawbacks: the recombination process occurs over a relatively large distance because of the carrier diffusion length leading to increased nonradiative recombination, and reabsorption of the light produced in the active region becomes stronger with an increased material cap layer length as shown schematically in Fig. 7.4a.

For increasing the intensity of the output light, heterojunction LEDs use a double heterostructure (DH) or a quantum well in the active region. The DH device is based on two junctions between different semiconductor materials with different

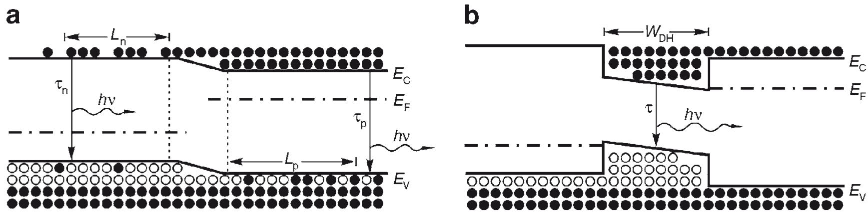

Fig. 7.4 Forward bias simplified energy band diagram for (**a**) homo and (**b**) double heterojunction

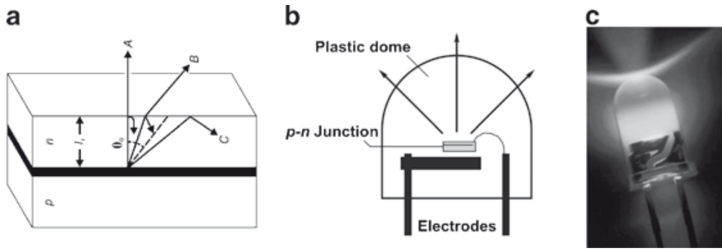

Fig. 7.5 (**a**) Light beam total internal reflection in the LED chip. (**b**) Cross section of a standard LED surrounded by plastic encapsulation. (**c**) Standard LED picture in plastic encapsulation

band gaps. The band structure and the distribution of injected carrier density under a forward bias in the DH device are shown schematically in Fig. 7.4b. There is a band gap change at the junction boundaries that results in a step-wise change in the bands creating an energy barrier that prevents diffusion of the injected carriers into the opposite region.

The performance of LEDs is best described by their ability to convert electrical energy to a luminous power. The power performance represents a value of the luminous power efficacy given by $F_v \Delta P_e$ [lm/W], where P_e is the power dissipated in the forward biased diode and F_v is the luminous flux [16]. The total light output power from the LED chip is never equal to the light power emitted from the active layer because light is emitted in random directions due to spontaneous emission as shown in Fig. 7.5a. The number of photons created by the spontaneous recombination in a unit volume of the active layer gives the internal quantum efficiency η_i. The internal quantum efficiencies of some direct band gap semiconductors can approach 100%. The reason of low external efficiencies η_e is the nontransparency of the substrate for visible light that results in photon absorption and mainly reflection of the emitted light at the chip surface as shown in Fig. 7.5a. Most of the emitted light strikes the material interface at an angle greater than the critical angle (C) and hence remains trapped. However, because of the large difference in the refractive index between the semiconductor and the air or surrounding encapsulant (n = 3.5 and 1 or 1.5, respectively), only light emitted in direction A, B within a cone of semiangle Θ_c (~16 for n = 3.5) will escape from the chip. So the external efficiencies of

conventional LEDs are limited to about 4% for each available semiconductor surface [17].

The basic LED consists of a semiconductor diode chip mounted in the reflector cup of a lead frame that is connected to electrical (wire bond) wires and then encased in a solid epoxy lens (Fig. 7.5b). The colored light of a LED is determined exclusively by the semiconductor compound used to make the LED chip and is independent of the epoxy lens color. Solid state design allows LEDs to withstand shocks, vibration, frequent switching (electrical on and off shocks), and environmental (mechanical shocks) extremes without compromising their famous long life, typically 100,000 h or more.

7.2.4 OLEDs Technology

In the last decades, conducting organic materials have attracted a lot of interest as new materials for electronic applications because of their several advantages over the conventional semiconductors. They offer the potential for low fabrication cost, easy processing, and flexibility. OLEDs, organic field-effect transistors (OFET), photodiodes, and solar cells are applications under intense study, and the first products is already in commercial use [18]. There has been a growing research effort in “organic electronics” to improve the semiconducting, conducting, and light-emitting properties of organics [19, 20]. Nontraditional materials such as conjugated organic molecules, short-chain oligomers, and small molecules are being developed such that they emit light, conduct current, and act as semiconductors. The ability of these materials to transport charge (holes and electrons) due to the p-orbital overlap of neighboring molecules provides their semiconducting and conducting properties. Recombination of charge carriers under an applied field can lead to the formation of an exciton that decays radiatively giving rise to light emission. Two main technologies for OLEDs have emerged in the last decade, either based on conjugated polymers or sublimed films of small molecules [21]. With a commercial history of just 7 years, OLED manufacturing remains at an early stage, both in terms of technique and equipment. Small-molecule OLEDs are made using vapor deposition techniques, such as evaporation through a shadow or integrated shadow mask because OLED materials are too delicate for photolithography. Polymer PLEDs are made by solution processing, either spin-on techniques (for monochrome) or inkjet printing (for colour), although the latter has not yet been commercialized.

The principle of operation of bilayer OLEDs is similar to that of inorganic LEDs, as shown in Fig. 7.6. Holes and electrons are injected from opposite contacts into the organic layer sequence and transported to the emitter layer. Recombination leads to the formation of singlet excitons that decay radiatively. In detail, electrons are injected from a low work function metal contact (cathode), e.g., Ca or Mg. The last one is chosen for the sake of stability. A wide-gap transparent indium-tin-oxide (ITO) thin film is used for hole injection (anode). The efficiency of electron–hole recombination leading to the creation of singlet excitons is mainly influenced by

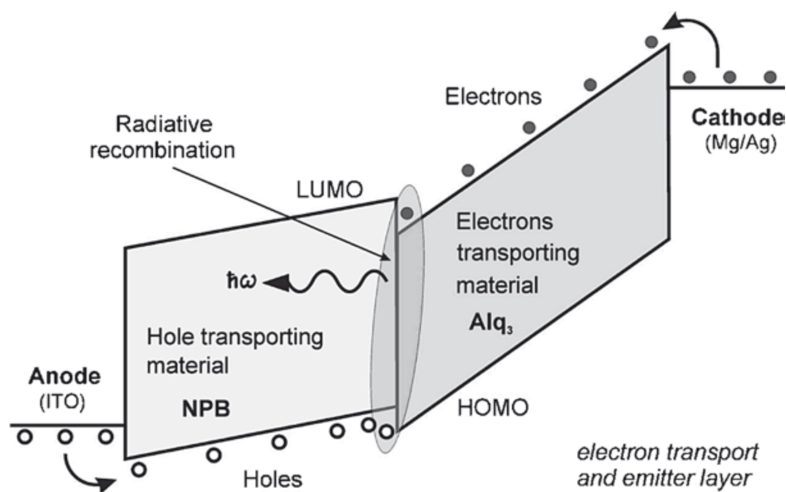

Fig. 7.6 Energy diagrams for bilayer OLED

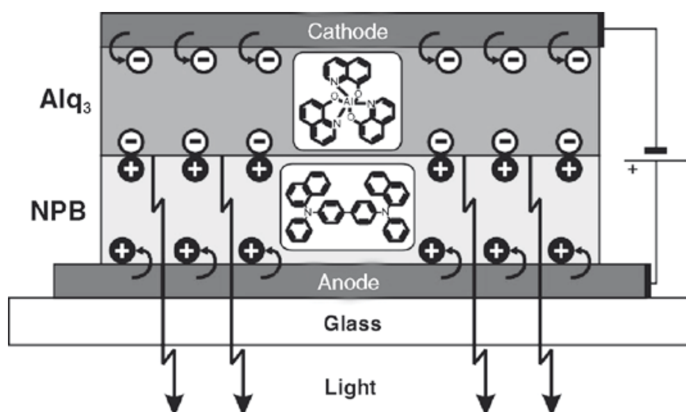

Fig. 7.7 NPB/Alq_3 bilayer OLED structure

the overlap of electron and hole densities that originate from carrier injection into the emitter layer. Schematic of a typical organic light-emitting diode, which uses Alq_3, tris(8-hydroxyquinolinato) aluminum, as the electron transport and emitting layer, and NPB, *N*,*N*′-di(naphthalene-1-yl)-*N*,*N*′diphenylbenzidine, as the hole transport layer, is depicted in Fig. 7.7.

As an example, the characteristic luminance, current density, voltage and spectral characteristics of bi-layer NPB/Alq_3 device are shown in Figs. 7.8 and 7.9 [22]. The luminance continuously increased with the increase in voltage and reached a value up to 1,000 cd/m^2 at 10 V showing typical Alq^3 spectral emission maxima at 530 nm. The turn-on voltage of about 4 V is mainly determined by the total layer thickness (60 nm NPB, 60 nm Alq^3) of green devices.

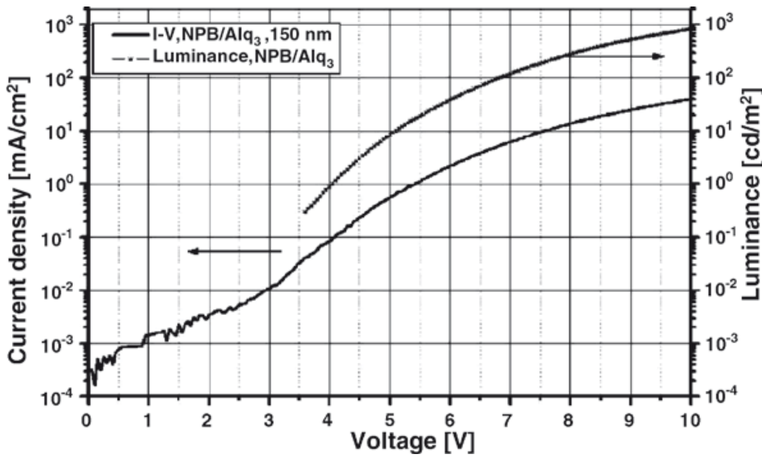

Fig. 7.8 Characteristic luminance-current density vs. voltage layer of bilayer NPB/Alq_3 device

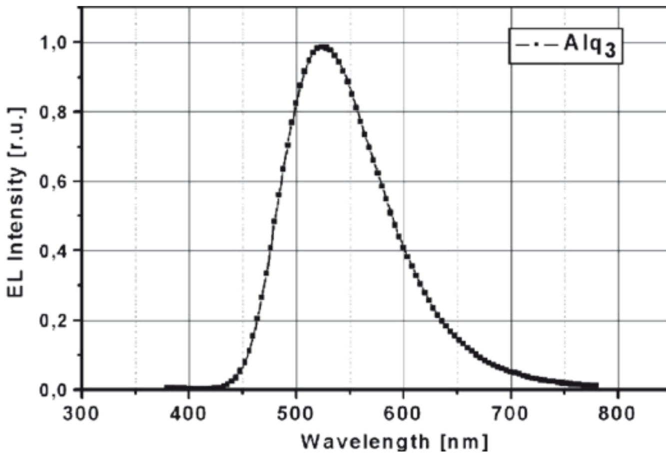

Fig. 7.9 Spectral characteristics of a bilayer NPB/Alq_3 device

7.2.5 Research and Development of LEDs on Graded Buffer

7.2.5.1 LED Simulation

The main engineering challenge in light generation efficiency of single source LED chips is now the extraction efficiency or the ability to get all the light out of the chip to where it is needed. This leads to a novel change, replacement of a gallium arsenide (GaAs) production wafer with transparent gallium phosphide (GaP) [23]. A new way to design LEDs can be the direct growth of InGaP or AlInGaP-based LEDs structure on a GaP substrate, using an $In_xGa_{1-x}P$ graded layer [24].

The LED structures grown on GaP substrate were designed and simulated using the APSYS -LED design software [25]. The multilayered $In_xGa_{1-x}P$ structure was designed as a sequentially grown graded buffer of 8 × 100 nm thick $In_xGa_{1-x}P$ layers with a change of $In_xGa_{1-x}P$ compositional value $D_x = 0.04$ per layer. The design of the graded region is necessary to bridge over the lattice mismatch between the GaP substrate and to reach composition over $x = 0.27$, where the ternary $In_xGa_{1-x}P$ is a direct band gap semiconductor as shown in Fig. 7.14. The design of a homojunction LED structure on a graded buffer consists of a 1-μm thick n-doped cladding layer with composition $In_{0.36}Ga_{0.64}P$ followed by an undoped 300-nm thick active layer and a 1.5 μm p-type layer. The simulated band diagram of the designed structure is illustrated in Fig. 7.10 for 0 and 2 V forward bias voltages. It is assumed that E_C, E_V, and E_g depend linearly on the composition x.

In the band energy diagram, one can distinguish the steps of the graded buffer as an interface between the wide band gap GaP substrate and the narrow-band gap $In_{0.36}Ga_{0.64}P$ layer.

In Fig. 7.11a, a simulated I-V characteristics of the designed LED structure is shown in linear and logarithmic scales. From the linear characteristics, the onset

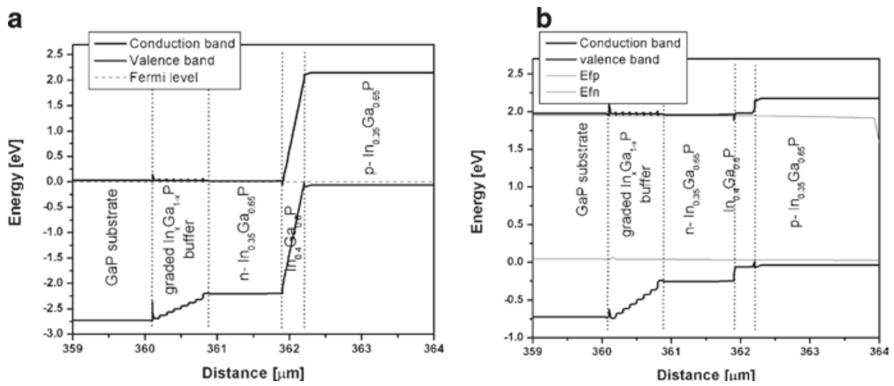

Fig. 7.10 Simulated LED structure band gap energy diagram (**a**) without and (**b**) with 2 V applied forward bias voltage

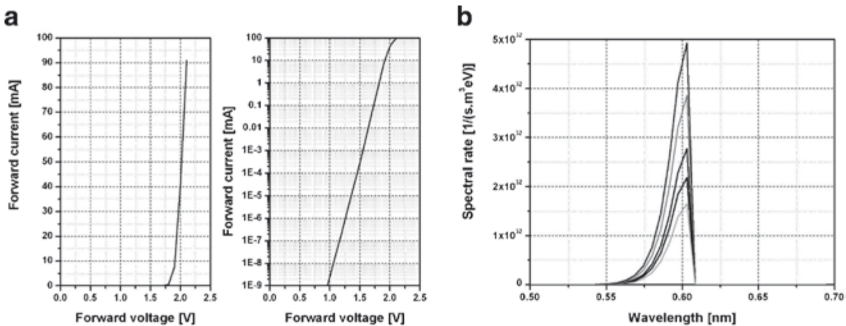

Fig. 7.11 Simulated (**a**) I–V and (**b**) spectral characteristics of the LED

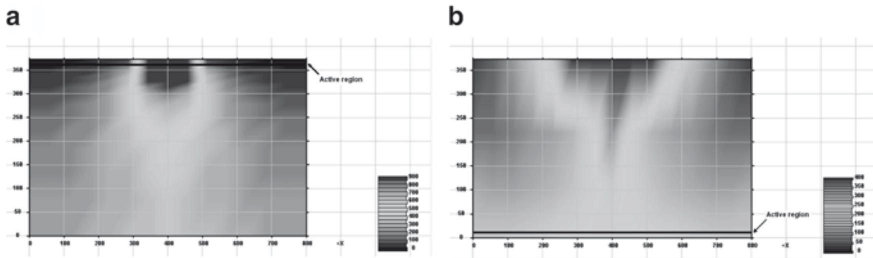

Fig. 7.12 Current spreading simulation of a LED structure, where a bottom full surface covering contact is placed (**a**) on the substrate and (**b**) on the active region side of the structure

voltage near 1.75 V needed for LED operation was determined. The simulated LED electroluminescence (EL) spectra for different driving currents in the range 10–50 mA (step 10 mA) are depicted in Fig. 7.11b. The EL spectra show the emission maxima at 605 nm for the designed homojunction LED containing an $In_{0.4}Ga_{0.6}P$ active layer. Variation of the active region thickness in the range of 300–700 nm has no significant influence on the emission intensity. For optimizing the LED structure contact, the current spreading in the LED structure was simulated, and the influence of the position of the contact covering the whole surface was analyzed. The device structure containing InGaP DH consisted of an undoped $In_{0.35}Ga_{0.65}P$ (500 nm) active layer inserted between n-$In_{0.15}Ga_{0.85}P$ and p-$In_{0.15}Ga_{0.85}P$ cladding layers with thickness 1 μm placed on the GaP substrate. The doping level of n and p-type cladding layers was 3×10^{18} cm^{-3}. Two simulations were made changing the position of the contact covering the whole surface, and the second shaped contact placed in the middle of the top side of a differently oriented LED chip. The width of the second contact was 200 μm. In Fig. 7.12a, b, the influence of the placement of the full surface contact is shown on the current spreading for LED chips in conventional and inverted structures, respectively. If the low area contact is on the active layer side of the chip, the current is flowing only through the narrow part of the active region as shown in Fig. 7.12a. Usually the substrate is the heaviest part of the LED structure, and in the case of its transparency, the substrate can act as a spreading layer. If the structure is inverted, which means that the top shaped contact is prepared on a GaP substrate, the current spreading problems in the narrow p-n part of device structures are eliminated because the full surface of the active layer is covered by an ohmic contact. In this case, the current density is equally distributed in the active region of the LED structure, which occurs at the bottom, as shown in Fig. 7.12b.

7.2.5.2 Growth and Characterization the LED Structure

An $In_xGa_{1-x}P$ graded buffer LED structure was grown by low-pressure IR-heated LP MO CVD on a sulfur-doped (100) GaP wafer. As precursors, phosphin (PH_3), trimethylgallium (TMGa), and trimethylindium (TMIn) were used. A 300-nm thick

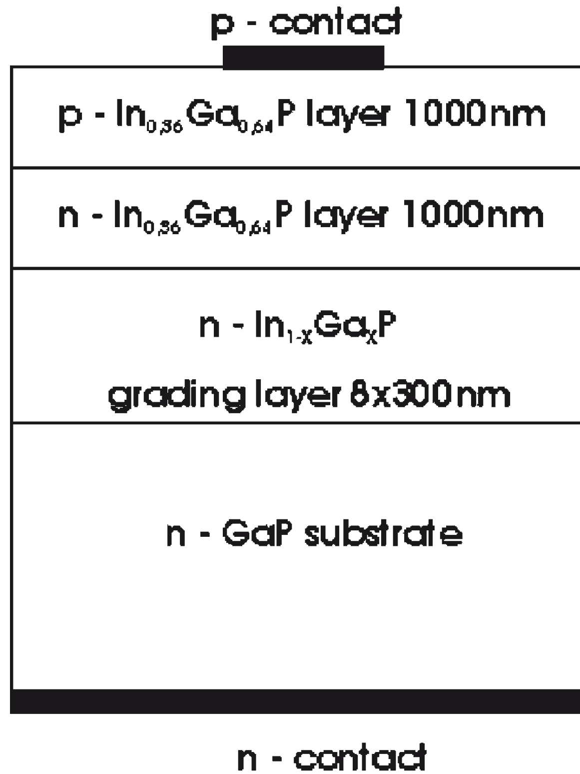

Fig. 7.13 InGaP-based homojunction LED directly grown on a GaP substrate

GaP Si-doped buffer layer ($n = 1.9 \times 10^{18}$ cm^{-3}) was deposited before the growth of the step-wise graded Si-doped $In_xGa_{1-x}P$ buffer. It consists of eight 300-nm thick $In_xGa_{1-x}P$ layers with compositional change $\Delta x_{In} \sim 0.04$ between the steps, as shown in Fig. 7.13. The role of this graded buffer is to change the lattice constant from the GaP substrate lattice constant value to the final active layer lattice constant while remaining able to filter dislocation propagation to the electroluminescent part of the LED structure, as depicted in Fig. 7.14. The growth conditions were described in detail in literature [26, 27].

On top of the graded buffer a homojunction LED structure was grown with equal 1-μm thick n and p layers of $In_{0.36}Ga_{0.64}P$ composition. The lattice parameter of the final layer in the buffer as determined by X-ray diffraction was 5.583 Å. The measured photoluminescence spectra at 300 K showed a peak position near 590 nm. Ohmic contacts to n-side (Ni/Au/Ge) and p-side (Pd/Be/Pd) of the LED structure were evaporated and afterwards annealed in a forming gas. A set of testing LED chips were prepared with surface area 500 × 500 μm^2 for measurements of electrical and optical properties.

Field emission SEM in the secondary electron mode was used to characterize the surface morphology of the prepared structures, and cross-sectional dislocation

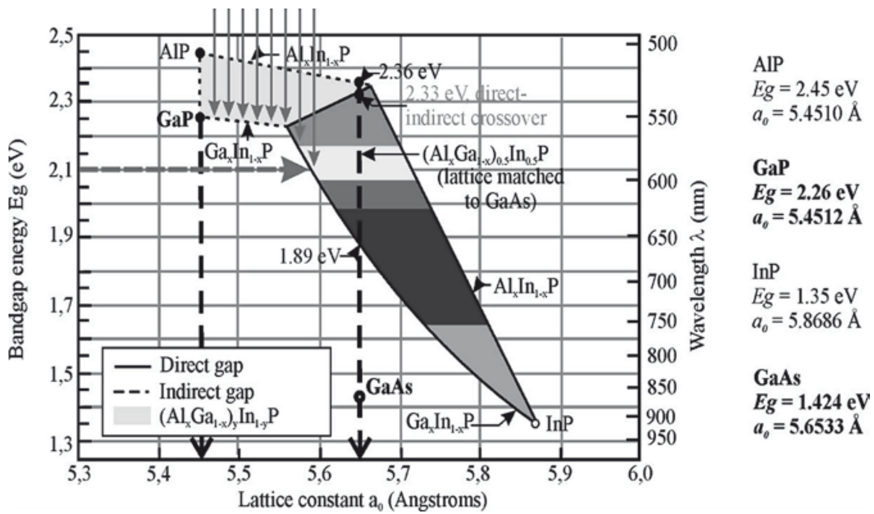

Fig. 7.14 Lattice constant and band gap energy variation with $In_xGa_{1-x}P$-graded buffer composition

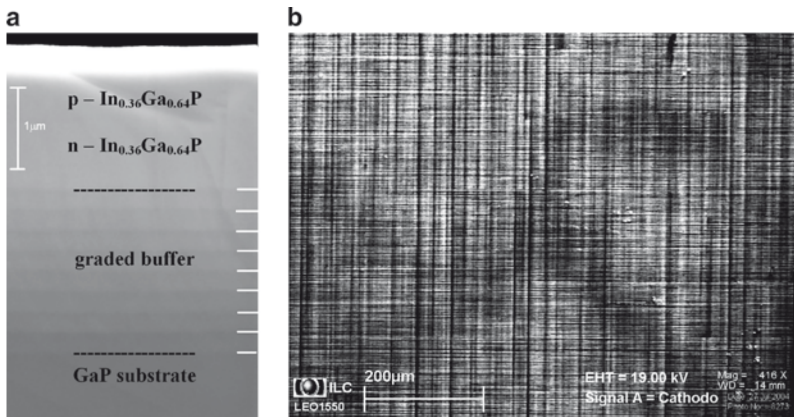

Fig. 7.15 (**a**) SEM image of the cleaved edge of the $In_xGa_{1-x}P$/GaP structure showing the graded buffer and the top homo-junction LED, (**b**) CL image of the top p-type $In_{0.36}Ga_{0.64}P$ layer

structure was examined by transmission electron microscopy. Figure 7.15a shows a SEM image of a cleaved edge of the $In_xGa_{1-x}P$/GaP structure. Starting points from the GaP substrate through individual grading, $In_xGa_{1-x}P$ interlayers and the homo-junction are clearly seen. No degradation in the cross-sectional SEM micrograph was revealed. The cathodoluminescence image plotted in Fig. 7.15b shows a top view of the sample, where crosshatch defects appeared due to the lattice mismatch and strain in the structure [28]. The total lattice mismatch is 2.37% between the

GaP substrate and top $In_{0.36}Ga_{0.64}P$ layer. The In content in the graded buffer was determined by secondary ion mass spectroscopy (SIMS) [29]. The SIMS depth profile of the graded buffer confirmed the expected compositional change $\Delta x_{In} \sim 0.04$ between the steps as documented in Fig. 7.16. The surface of the LED structure suffers from crosshatch defects due to the high lattice mismatch and strain in the graded layers. This effect is observable on EL emission from the LED chip under optical microscope, as shown in Fig. 7.17.

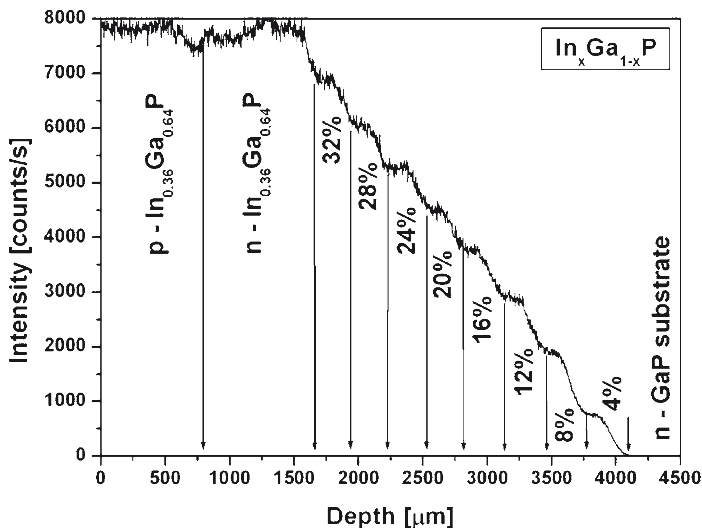

Fig. 7.16 SIMS depth profile of $In_xGa_{1-x}P$ from the graded buffer

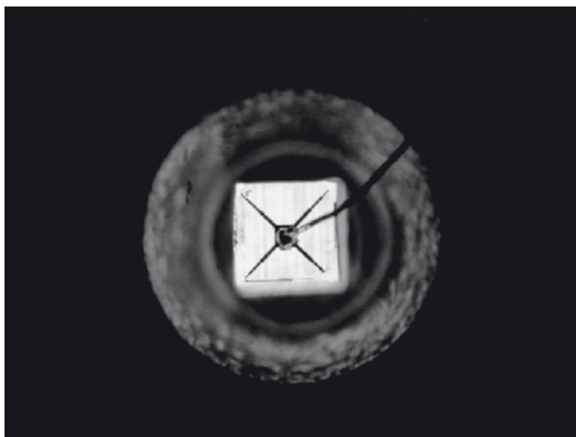

Fig. 7.17 Image of LED chip light emission

The I-V characteristics of realized InGaP/GaP LEDs are depicted in Fig. 7.18a and compared with an LPE grown green GaP LED (dashed line). The I-V curve of the analyzed InGaP structure shows an identical behavior with a GaP LED corresponding to the decreased band gap and turn-on voltage in the range of 1.7 V [28]. Different behaviors appear in the low current region due to an increased leakage current probably through dislocations in the structure. For the inverted structure, which means that the top contact was prepared on the GaP substrate, the leakage current decreases at low voltages. Moreover, current spreading problems in the narrow p–n part of the device structures were also eliminated because the whole surface of the p-InGaP layer is covered by the ohmic contact. Hence, it results in total current spreading and homogenous emission from the active region of the diode structure as well as improvement of light emission generation, as clearly seen in Fig. 7.17. An improvement of light emission by a factor of 1.5 was reached in comparison with device configuration in which the full surface covering contact was placed on the GaP substrate. Figure 7.18b shows a typical electroluminescence (EL) spectrum of the investigated InGaP homojunction LED measured at 300 K. All the measured EL emission spectra peaks are located at around 593 nm (at 20 mA), and the full width at half maximum (FWHM) was 25 nm, which is typical for a high quality InGaP layer corresponding to the calculated $In_{0.36}Ga_{0.64}P$ composition [28] (2.091 eV). A small red shift 6 nm was obtained in the range of driving currents from 10 to 50 mA. This is due to the band gap shrinkage caused by Joule heating.

The results obtained from InGaP LED show a promising emission intensity comparable with conventional GaP LEDs and a single emission peak near 593 nm with FWHM value of 25 nm corresponding to $In_{0.36}Ga_{0.64}P$ composition. We have demonstrated the capability of growing an $In_{0.36}Ga_{0.64}P$ homojunction LED on a GaP substrate, using an $In_xGa_{1-x}P$-graded interlayer. The research work was supported by EC project VGF GaP LEDs – focused on the development of "New GaP substrate grown by VGF method for LEDs."

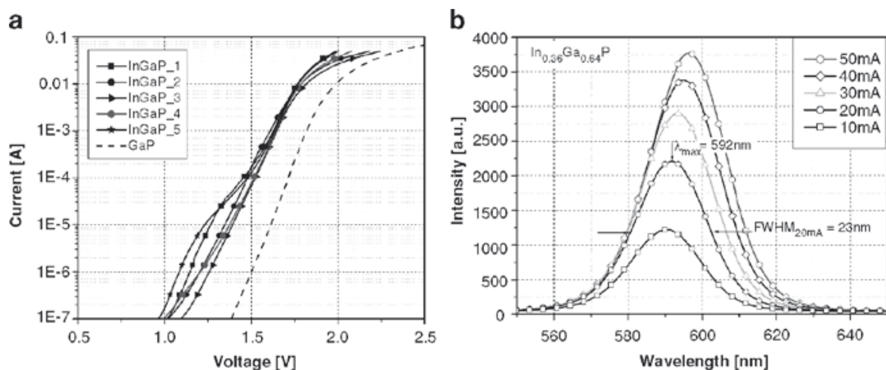

Fig. 7.18 Measured LED (**a**) I–V characteristics and (**b**) EL spectra at various forward currents

7.2.6 LEDs and OLEDs Recent Development and Trends

LEDs are among the most widely used semiconductor optoelectronic devices. Improvements in manufacturing the epitaxial material and packaging have enhanced the thermal conductivity and increased the overall light extraction efficiency of LEDs. Significantly, the light generation efficiency of these single-source LED chips has improved. Today's quantum efficiencies are very high so that the main engineering challenge is now the extraction efficiency or the ability to get all the light out of the chip to where it is needed. There even appears to be a LED version of the silicon industry's "Moore's Law" in which LED brightness doubles every 18 months [30]. In general, visible LEDs can be divided into two categories: "conventional" or low brightness, and new high brightness LEDs (HB LEDs). Conventional LEDs are found in any electronics, ranging from an indicator light up to an alpha numeric display. Most of the markets are well served by commercial LEDs, and they do not need to have high brightness. Conventional LEDs are based on homojunction devices that can be relatively inexpensively produced using older liquid phase epitaxy (LPE) and vapour phase epitaxy (VPE) growth techniques. The majority of HB LEDs are based on AlGaAs/GaAs, AlInGaP/GaAs, and InGaN/GaN heterojunction devices produced by MOCVD. Significant improvements in producing AlInGaP and InGaN structures have enhanced the brightness, specifically in green and blue LEDs. In Fig. 7.19, the LEDs evolution roadmap is illustrated showing the rate of improvement in performance of about tenfold increase in

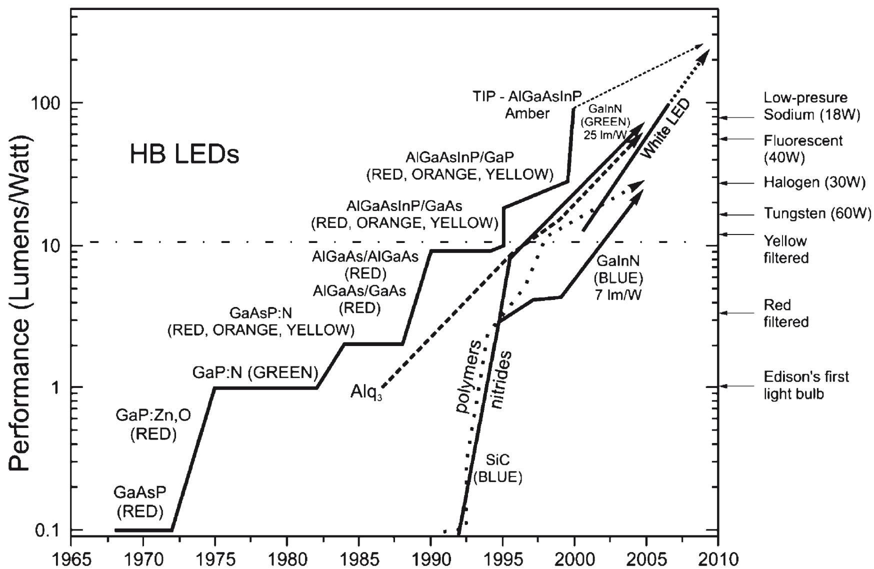

Fig. 7.19 Evolution of LEDs and OLEDs performance

light output per decade. The first LED was developed in 1960 based on GaAsP layers. Development of $A^{III}B^{V}$ compound semiconductors technology and their ternary and quaternary alloys incorporated in LED structures rapidly increased the performance. Recently, fabricated LEDs using double heterojunction (DH) or MQWs active layers increased their efficiency several times [21].

Development of HB LEDs is roughly divided to two main orientations: first using $(Al_xGa_{1-x})_{0.5}InP_{0.5}$ active layer lattice matched to GaAs (covering amber to red color), and the second, $GaN/In_xGa_{1-x}N$ nitride based technology (covering blue to green colors). LEDs using AlGaInP quaternary were developed in the mid nineties using a GaAs substrate, and their performance reached a value of ~12 lm/W. Disadvantage of this substrate is its nontransparency for visible light, which results in photon absorption by the substrate. To resolve this problem, the wafer bounding technique was used. In the wafer bonding technique, after selective etching of AlGaInP epilayers, the highly transparent GaP substrate is placed in contact with LED epilayers. Therefore, improving the light extraction is a major issue in fabricating high-efficiency LEDs [31]. Changing the absorbing substrate to a transparent one doubles the flux output from the same epitaxial structure. Using a different shape of the previously mentioned LED structure called a truncated-inverted-pyramid (TIP), the performance reaches 100 lm/W for amber light [32]. Recently, the major development is concentrated on increasing the brightness of nitride-based LED devices. The wider band gap of nitride semiconductors filled the wavelength gap between the common red-orange-yellow LEDs and the nonvisible near UV region [33]. GaN, AlGaN, and InGaN layers are grown by MOVPE on a sapphire or SiC substrate. The active $In_xGa_{1-x}N$ layer covers the band-gap energy in the range of 1.95–3.4 eV. All structures include a buffer layer because the interface between the surface and the nitride layer contains many dislocations (the lattice mismatch is 3.5% for SiC and 13% for sapphire) [6]. Sapphire is inexpensive and highly transparent while SiC gives many advantages from the epitaxial growth and device processing point of view. The main goal in nitride technologies is to increase the performance above 100 lm/W and to use blue HB LEDs as a basic light source in high brightness white light devices [34].

There are three basic approaches to making white light using LEDs. One is to combine the output from two or more LED chips; these could be blue and yellow, or more commonly red, green, and blue (RGB). The second approach is phosphor conversion, in which a blue LED chip is combined with a phosphor. Some of the blue photons are down-converted by the phosphor to produce a broad emission centered on yellow; this mixes with other blue photons to create white. The third main approach is to use a UV LED as a pump chip for a mixture of phosphors that emit across the visible spectrum [35].

Enhancements in performance have been seen in the development of OLEDs. Figure 7.19 shows the dramatic increase in the luminous efficiency of light-emitting molecular solids and polymers compared with typical inorganic LEDs over a 15-year time scale [7]. Pioneering work was done at Eastman Kodak on evaporated small molecules (Alq_3) in 1987 [36] and at Cambridge University on solution-processed semiconducting polymers in 1990 [37]. Currently, the highest

observed luminous efficiencies of derivatives of these materials exceed that of incandescent light bulbs, thus eliminating the need for the backlight that is used in AMLCDs. The electronic and optical properties of these "active" organic materials are now suitable for some low performance, low-cost electronic products that can address the needs for lightweight portable devices. Through its application, a thin display that does not require backlight can be realized. The expectation is high, such as replacement for flat panel displays in mobiles. Development is in progress with the view toward using it in TV sets in the future. There is a hope for the organic EL elements to provide new forms in displays that did not exist before, such as forming them on plastic sheets and making them as flexible films. OLED, OLED displays, organic field effect transistors (OFET), photodiodes, and solar cells are applications under intense study, and the first products are already in commercial use. The steadily growing interest in OLEDs currently focuses on three major fields of applications: lightning/signature, passive-matrix displays for portable players and mobile phones, as well as active-matrix displays for computers and television screens [38].

In recent years, major advancements in LED technology have been achieved, such as developing a new technology that increases the LED light output by as much as 20 times over earlier generations, and allows production of daylight-visible LEDs virtually in any color of the spectrum. Even white light, long thought to be an impossibility, is now available in three different shades as a light-emitting diode. Over the past decade, LEDs performance has steadily improved until it exceeds that of incandescent lamps. If this progress continues, LEDs also will outperform fluorescent lamps and will be the primary sources for general illumination [39]. Recent improvements in the light output have enabled also new applications for LEDs such as automotive lightning, traffic signals, and more recently television displays [3, 40].

A very rapid progress was made over the last few years in developing organic semiconductor devices.

7.2.7 Photodetectors for Optical Communications

7.2.7.1 Photodetectors Basic Concept

If light of a proper wavelength is incident on the depletion region of a *p-n* junction diode while a reverse voltage is applied, the absorbed photons can produce additional electron–hole pairs. This yields a photocurrent in addition to the diode current so that the total diode current is given by $I = I_0 \exp[(eU / k_b T) - 1] - I_{ph}$, where the additional photocurrent, I_{ph}, is due to photogeneration of electrons and holes. The maximum photocurrent in a photodiode equals $I_{ph} = \eta_q (e\lambda / hc) P_{in}$, where η_q is the quantum efficiency and P_{in} is the incident optical power. The quantum efficiency is the ratio of the number of generated *e-h* pairs and incident photons.

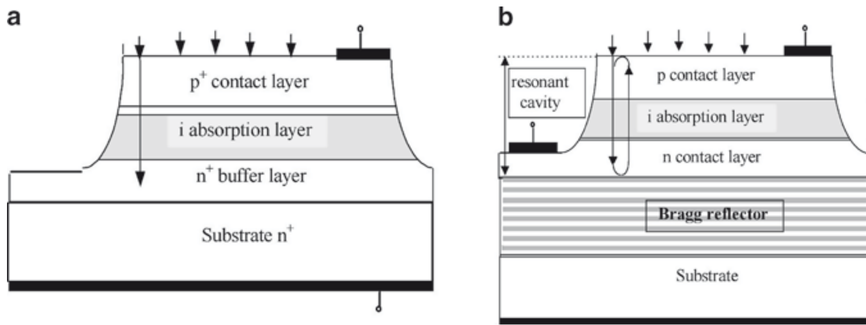

Fig. 7.20 (**a**) *p-i-n*, (**b**) RCE *p-i-n* photodetector

The responsivity (R) of a photodiode characterizes its performance in terms of the photocurrent per incident optical power at a given wavelength and is given by $R = I_{ph}/P_{in}$ (A/W).

Reverse-biased p–i–n diodes are probably the most widely used photodetectors for optical communications [8, 9]. Schematic structure of a p–i–n photodetector is shown in Fig. 7.20a. In such a structure, the electrons and holes are generated by absorbed light in the undoped region and separated by the built-in electric field toward the electrodes. Efficient detection of the incident optical power requires that maximum of the light is absorbed within the intrinsic region. The p–i–n photodiodes can achieve quantum efficiencies of up to 80%. The response time of photodiodes is limited by two factors: the finite transit time of carriers across the depletion region, and the RC time constant associated with electrical parameters of the diode and its external circuitry.

RCE photodetectors are optoelectronic devices whose performance is enhanced by placing the active device structure inside a Fabry-Perot resonant microcavity as shown in Fig. 7.20b. Such RCE devices benefit from the wavelength selectivity and the large increase of the resonant optical field introduced by the cavity. The increased optical field allows photodetectors to be made thinner and therefore faster, while simultaneously increasing the quantum efficiency at the resonant wavelength.

Avalanche photodiodes (APDs) are used in optical communications because of their high speed and internal gain. An avalanche photodiode is a specially designed reverse biased photodiode in which an incoming light signal initiates an avalanche breakdown. When the reverse bias is increased sufficiently, avalanche occurs and the optically generated photocurrent is amplified. Hence, carriers generated by light create other carriers via impact ionization, providing an internal gain. APDs use special design features to prevent edge breakdown. They exhibit a high gain and high speed, with response times as short as several tens of picoseconds.

7.2.8 RCE Photodetectors

7.2.8.1 Design of RCE Photodetectors

RCE photodetector consists of a photodetector enclosed in an optical resonator, a resonant cavity of the Fabry-Perot type (Fig. 7.20b) [41, 42]. On the one hand, photons with wavelength corresponding to the resonance of the cavity are reflected back by the mirrors and pass the cavity multiple times, increasing the probability that they will be absorbed in the active layer of the detector. The sensitivity of the detector at the resonant wavelength is hereby increased compared with a similar structure without a resonator. On the other hand, photons with wavelengths different from the resonant wavelength are reflected back from the surface. As a consequence, sensitivity of the detector is suppressed at these wavelengths compared with a similar structure without a resonator. The resonant wavelength depends on the optical length of the cavity

$$\lambda = \frac{L_{\mathrm{eff}} n}{k}, \tag{7.1}$$

where L_{eff} is the effective length of the cavity including the penetration depth to the mirrors, n is the refractive index of the cavity material, and $k = 1, 2, 3$ is the order of resonance. The spacing between adjacent resonant wavelengths is

$$\Delta\lambda = \frac{\lambda^2}{2nL_{\mathrm{eff}} + \lambda}. \tag{7.2}$$

With an increasing length of the resonant cavity this spacing decreases, and for long cavities more than one resonant peak can occur within the reflectivity window of the Bragg reflector. Usually the material of the resonant cavity is chosen so that there is no significant absorption in the cavity except in the active layer.

7.2.8.2 Semiconductor Bragg Reflectors for 855 and 1300 nm Wavelength Ranges

The structure of RCE photodetectors consists of layers of different materials grown on each other by MBE or MO CVD. All materials should be able to grow on each other; usually lattice matched to one of the common substrate materials (GaAs or InP). From the electrical point of view, the materials should be dopable to both types in required concentrations, and they should have a low defect rate. Materials for intrinsic layers should have low background doping concentrations, and the contact layer materials should be able to create ohmic contacts with metals. The material for the cavity itself and for the Bragg reflector should have the lowest possible absorption at the design wavelength, while the material of the active layer should be absorbing at the same wavelength. In other words, materials for the

cavity and for the Bragg reflector should have the band gap energy higher than the energy corresponding to the working wavelength, while the active layer material band gap energy should be below that. Additionally, the refractive index contrast for the Bragg reflector materials should be as high as possible [41].

AlGaAs/GaAs is the most popular material system for investigation of the heterostructures. This is due to the following factors: historically, GaAs was one of the first $A^{III}B^{V}$ compound semiconductors studied, and the commercial success of the GaAs/AlGaAs heterojunction-based transistors and the first semiconductor LDs boosted the research and development of this material system. GaAs substrates are available in high quality (low defect density), at low cost and with large diameters (up to 6"). AlGaAs can be grown on GaAs substrates by MBE as well as by MO CVD almost lattice matched at any fraction of Al, providing materials with band gap ranging from 1.424 eV for GaAs (direct band gap) up to 2.17 eV for AlAs (indirect band gap), in terms of absorption edge, 870–570 nm, respectively. The AlAs/GaAs material combination exhibits the highest refractive index contrast amidst practical semiconductors for a wide range of wavelengths (n_{GaAs}/n_{AlAs} = 3.5/2.95 at $\lambda = 1$ μm, 3.4/2.9 at $\lambda = 1.3$ μm, 3.37/2.89 at $\lambda = 1.55$ μm), making this material combination attractive for Bragg reflector design. A high reflectivity Bragg reflector can be obtained using a small number of layers, and the high reflectivity wavelength band is relatively wide.

The band gap range limits the utilization of this material system to the wavelength range below 870 nm. This is a serious drawback in optical communications, as the absorption of the glass fiber is relatively high at these wavelengths. However, for shorter interconnections, optical local area networks (OLAN), and for very short interconnections (on-chip, chip-to-chip, board-to-board), the 850-nm wavelength region still remains the choice because of the advantages mentioned earlier.

The most commonly used material systems for $\lambda \sim 850$ nm are AlAs/GaAs and $Al_xGa_{1-x}As$/AlAs. The highest refractive indices difference $\Delta n \sim 0.6$ is between AlAs and GaAs. For modeling the optical properties, such as reflection, transmission, and absorption in structures consisting of stacked planar layers of optically homogeneous materials, the transfer matrix technique was used [43]. However, GaAs is absorbing for the wavelength of 855 nm and a nonabsorbing mirror could be made of an $Al_{0.3}Ga_{0.7}As$/AlAs quarter wave stack. Figure 7.21 shows the dependence of the maximum mirror reflectivity on the number of $Al_xGa_{1-x}As$/AlAs pairs. With 20 pairs a reflectivity of 99% could be achieved, and it remains constant in the wavelength range 830–880 nm. Figure 7.22 shows the calculated reflectivity spectra of 20 pairs of $Al_{0.3}Ga_{0.7}As$/AlAs for the 855 nm wavelength range [44].

The most important material system for optical communications is the heterostructure based on InP/InGaAsP quaternary material system. The invention of MO CVD greatly enhanced the development of epitaxially grown phosphide compounds, mainly on InP substrates. InP substrates are substantially more difficult to prepare, hence more expensive and of lower quality than GaAs substrates. However, the variety of materials that can be epitaxially grown lattice matched on InP gives it a superior position for optoelectronic devices operating at 1.3 and 1.55 μm

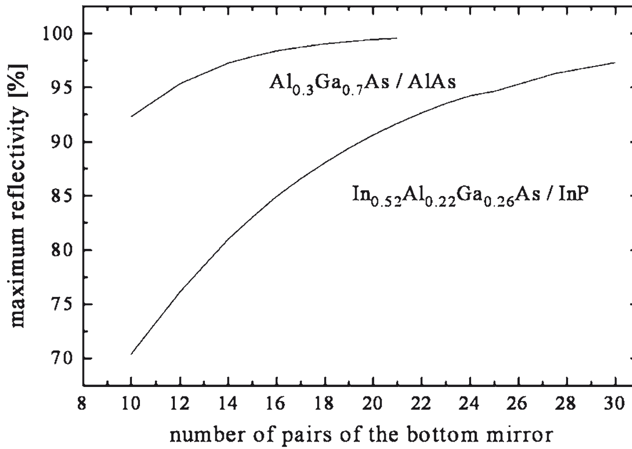

Fig. 7.21 Maximum reflectivity vs. the number of pairs of mirrors

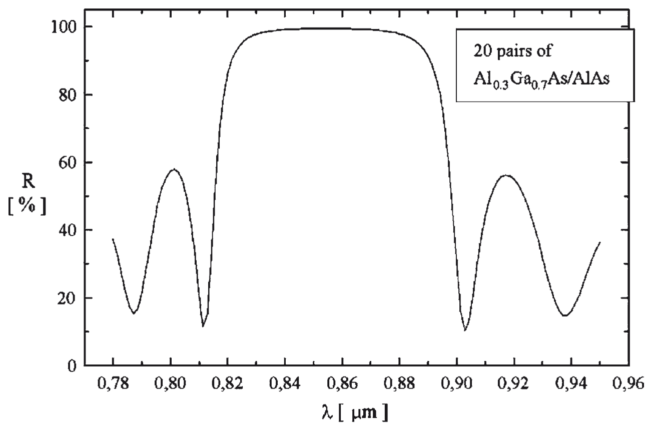

Fig. 7.22 Simulated reflectivity spectra of an AlGaAs/GaAs mirror

wavelength ranges. Ternary and quaternary compounds of In, Ga, Al (Group III), As, and P (Group V) elements provide an infinite variation of materials with a varying refraction index and absorption edge corresponding to the band gap energy. Although quaternary compounds such as InGaAsP or InGaAlAs provide more degrees of freedom in choosing materials for a given working wavelength, generally they are more difficult to prepare, as the ratio of more components should be controlled carefully. Materials lattice matched to InP exhibit a rather small

refractive index contrast (e.g., $n(In_{0.63}Ga_{0.37}As_{0.8}P_{0.2})/n(InP) = 3.42/3.17$ at 1.55 μm). Consequently, Bragg reflectors require a big number of layers, making their growth expensive and time consuming.

For the wavelength range over 1.3 μm, a typical material system is $In_{1-x-y}Al_xGa_yAs$/InP. Since the refractive indices difference is smaller than for AlGaAs/AlAs system, more pairs must be grown to get the high reflectivity. For comparison, the maximum reflectivity vs. the number of pairs of $In_{0.52}Al_{0.22}Ga_{0.26}As$/InP mirror designed for 1.3 μm is plotted in Fig. 7.21 as well. In this case up to 30 pairs are necessary to give a reflectivity of 97%. The difference in refractive indices is increasing with the increasing content of Al but at the same time the energy gap is decreasing and the mirror would be absorbing.

7.2.8.3 Tunable MQW RCE Photodetector Design and Characterization

In many systems, it is required to tune the components to a particular wavelength. Tunability of the RCE photodetector can be obtained by replacing the (wide spectrum) absorbing layer of the detector by a multiple-quantum well (MQW) structure [45].

In RCE MQW structures, the excitonic peak enhanced by the resonator provides wavelength selectivity and the quantum confined stark effect (QCSE) provides tunability. The tunnability based on QCSE can be utilized because the excitonic absorption peaks shift to red with an increasing field in MQW region. As exciton absorption decreases in amplitude with an increasing electric field, this effect is compensated by the optical gain of the resonant cavity. The optical resonator cavity should, therefore, be of relatively low quality so that the enhancement peak is relatively wide and a single Bragg reflector structure is sufficient [44].

An electrically tunable RCE photodiode based on the QCSE in GaAs/AlGaAs MQWstructure for the 855 nm wavelength region was grown by MOCVD [46]. The optical resonator in the designed structure of RCE MQW is formed by 15.5 pairs of the bottom AlAs/$Al_{0.2}Ga_{0.8}As$ Quarter-Wavelength Stack Bragg reflector on the substrate side and the natural semiconductor-air interface on the top of structure (Fig. 7.23). The Bragg reflector broad reflectivity maximum is centered at 855 nm. The absorber is an undoped GaAs/$Al_{0.3}Ga_{0.7}As$ MQW structure with 20 GaAs wells of 9.5-nm thickness. The thickness of the adjacent $Al_{0.3}Ga_{0.7}As$ layers is calculated so that the enhancement maximum occurs at 855 nm. The top GaAs cap layer should be kept very thin to avoid significant absorption. Test diodes were fabricated from the designed sample. The measured spectral photoresponse of the prepared RCE MQW PIN photodiodes for different reverse voltages is shown in Fig. 7.24.

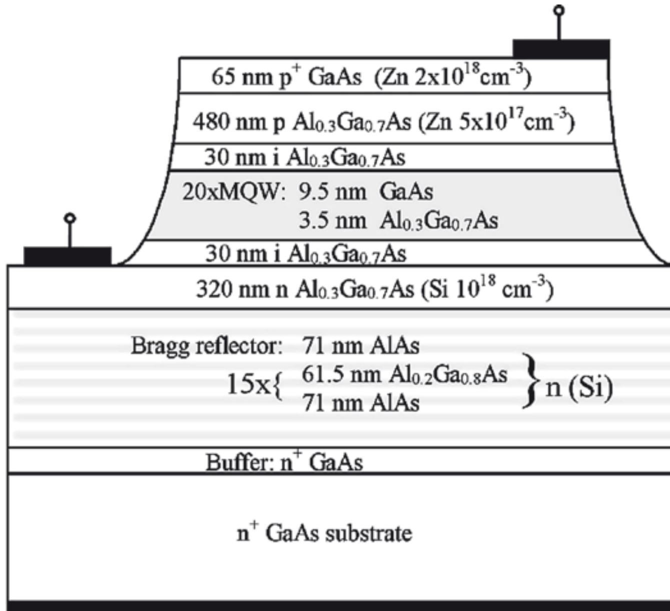

Fig. 7.23 Structure design of RCE MQW *p-i-n*

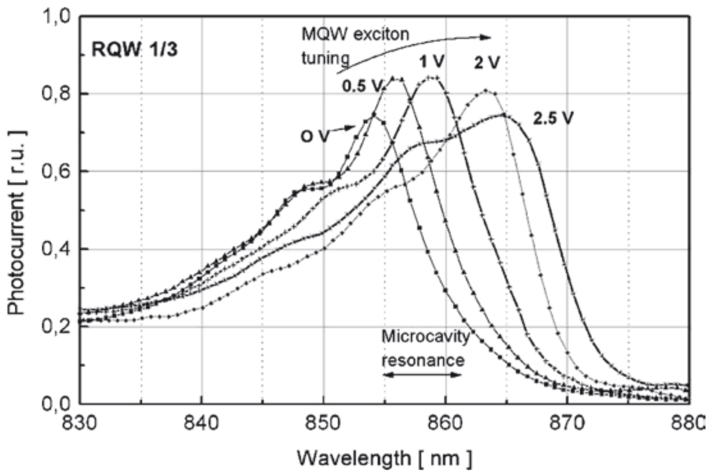

Fig. 7.24 Spectral photoresponse of tunable RCE

The tuning range of 12 nm at 2.5 V of the applied reverse bias was obtained for a structure with one bottom Bragg reflector and the physical principle of tuning based on the Quantum-Confined Stark Effect in the GaAs/AlGaAs MQW absorber was verified [44, 46].

7.2.9 Design and Characterization of Separated Absorption, Charge, and Multiplication (SACM) InGaAs/InGaAsP/InP APD Structure

An InGaAs/InP avalanche photodiode (APD) with a sectional InGaAsP/InP charge layer at the heterointerface between the InGaAs absorption and InP multiplication region has been designed, fabricated, and tested [47, 48]. Cross-sectional view of the designed SACM APD structure is depicted in Fig. 7.25a. In this design, long wavelength infrared light is absorbed in a narrow band gap material ($In_{0.47}Ga_{0.53}As$), while the photogenerated carriers are transported to and multiplied in a wider band gap (InP) material capable of sustaining high electric fields for providing an internal avalanche gain. The design was focused on the investigations of the electric field distribution in separated absorption, charge, and multiplication (SACM) APD layers in dependence on their doping concentration and thickness. The APSYS software was employed for simulations of the electric field distribution, carrier concentration, thickness of layers, and current–voltage characteristics of the designed APD structure at low voltages. The electric field distributions in the structure under different reverse bias voltages are depicted in Fig. 7.25b. The electric field in the central active region of the junction is enhanced by a selectively increased charge density under that region. The simulation results revealed that the sectional charge layer could be used to control the electric field profile in the APD structure.

The designed structure was grown by MOCVD in a single step on n-InP substrate. The test samples have been fabricated using standard photolithography, wet chemical etching, and lift-off ohmic contacts processing. For connecting the mesa diode (40 μm in diameter) top ohmic contact with a bounding pad, a gold air bridge

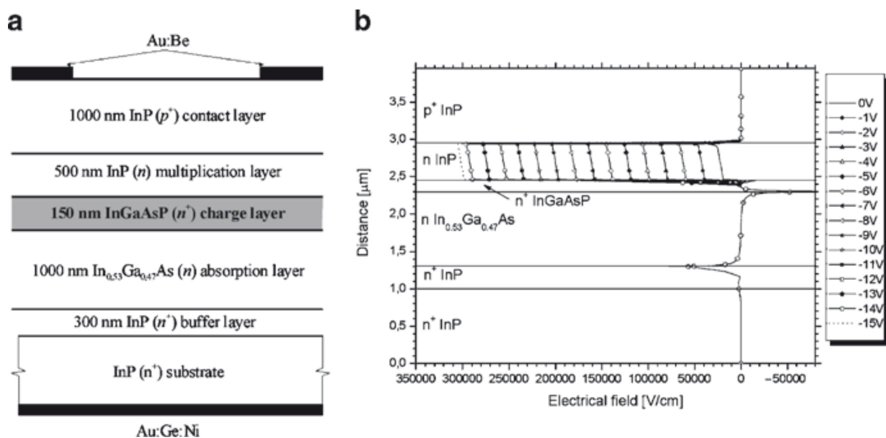

Fig. 7.25 SACM APD device: (**a**) Cross-sectional view, (**b**) Simulated electrical field distribution in the structure for different reverse bias voltages

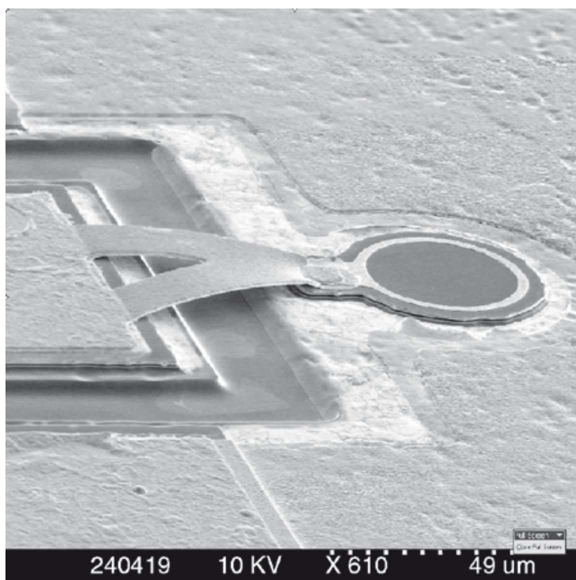

Fig. 7.26 *Top view* SEM image of processed photodiode

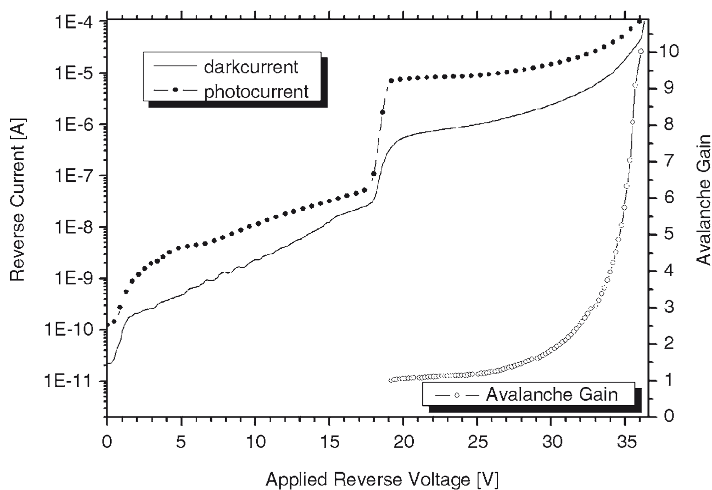

Fig. 7.27 I–V dark current and photocurrent characteristics

was formed as shown in Fig. 7.26. Dark current and photocurrent I–V characteristics under 1310 nm calibrated source illumination are shown in Fig. 7.27. The measured step in the I–V characteristics near 19 V is due to an extension of the electric field into the absorption layer.

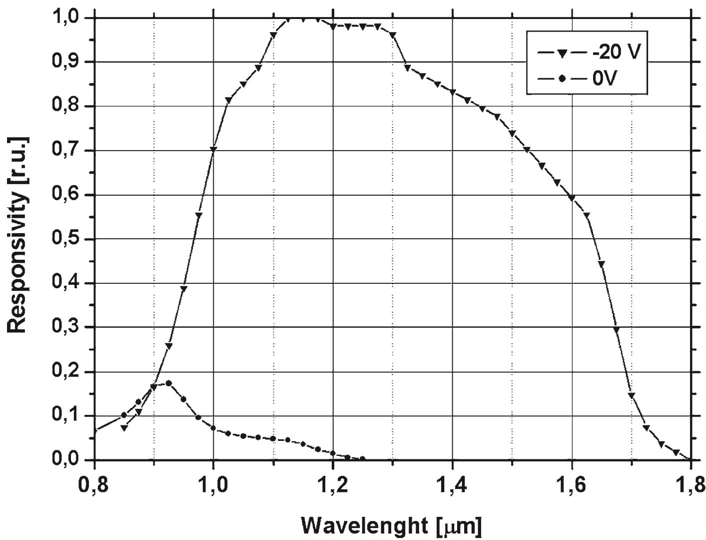

Fig. 7.28 Spectral characteristics of SACM APD at different reverse bias voltages

Within this mode of operation, the entire charge sheet and absorption layer are depleted. By increasing the bias voltage over 25 V, the carriers generated within the InGaAs absorption layer can drift into the multiplication region with high electric field thus providing an internal gain. Figure 7.28 shows the photodiode spectral characteristics at applied reverse bias voltages of 0 and 20 V. The SACM APD spectral sensitivity at reverse bias up to 15 V is low and corresponds to generation of carriers in the InP multiplication and InGaAsP charge regions. For the reverse bias voltage over 18 V, the depletion region is extended into the absorption layer and the device operates similarly as a p-i-n photodetector. At bias voltages higher than 25 V the sensitivity increases providing an internal avalanche gain. The measured photoresponse of the photodiodes without antireflection coating at 1310 nm was evaluated as 0.85 A/W at reverse voltage 20 V. Avalanche gain up to 10 was reached near the breakdown voltage of 35 V for designed SACM APD by utilizing an InGaAsP sectional charge layer.

7.2.10 Recent Developments in Optical Communications

In particular, microcavity devices such as VCSELs, RCE LEDs, and RCE photodetectors have recently received increased interest in optical interconnect technology. An ingenious concept for increasing the transfer rates of existing and future optical links is the WDM, where data are transmitted by light of different wavelengths simultaneously via the same optical fiber. RCE photodetectors represent a convenient solution for simple WDM receivers because of their inherent wavelength selectivity and potential for very high speeds [41].

Emerging optical interconnection technologies offer also a new capability. These novel technologies include parallel optics, high bandwidth plastic optical fibers, and new VCSELs, which cover an increasing range of wavelengths. Parallel optics offers low-cost interconnection with perhaps the best use of the backplane space. Plastic optical fibers (POF) have been demonstrated with high bandwidths above 1 GHz km and low loss between 850 and 1300 nm [1].

GaAs-based VCSELs are the dominant technology in transmitters for high performance, short-range data links, and optical network switches because of their low cost, ease of fiber coupling, and straightforward fabrication of large multielement 2D arrays. Unfortunately, these lasers operate only at 850 nm because of materials limitations. This short wavelength operation limits the system performance due to the wavelength-dependent dispersion and loss properties of silica fibers. The cost structure for high-density metro systems will require long-wavelength VCSELs and VCSEL arrays, which can be directly modulated, operated uncooled in ambient conditions, and produced at low cost. Such long-wavelength VCSELs will be the key elements in the next generation high-bandwidth data communication systems [49].

Avalanche photodetectors are preferred in long-haul and high bit rate transmission systems since they offer an improvement of the receiver sensitivity by several decibels [50, 51]. For APDs based on InGaAs/InP heterostructures, a higher carrier multiplication can be achieved in wider band gap InP layer. When the absorbing ternary layer is separated from the binary multiplication layer by an intermediate band gap or a graded quaternary layer, this structure is known as separate absorption and multiplication (SAM) or separate absorption, grading, and multiplication (SAGM) APD [52, 53]. To obtain a high gain-bandwidth product, the doping level and thickness of the multiplication layer must be very carefully controlled [54].

7.3 Silicon Photonics

The rapid development of microelectronic circuits over the past 50 years had a significant impact upon modern society. This is now the basis of complex microprocessors, large memory circuits, and other digital and analog electronics. Silicon as the most important material in the field of microelectronics is associated primarily with electronic devices. Silicon photonics in general means the use of silicon-based materials for generation, guidance, control, and detection of light to communicate information [55]. As silicon has proven to be cost-effective for the fabrication of integrated circuits, building optical devices on a silicon platform is considered a major thrust for the next generation of optoelectronic-integrated circuits. Implementation of silicon-based photonic devices, maybe even electrically pumped silicon lasers and silicon amplifiers [56, 57], could possibly lead to much smaller and cheaper photonic devices, making accessible a range of applications which so far have been impossible already for the reasons of too high costs [58].

Currently, a question of high interest is whether the silicon technology platform can also be effectively utilized in the area of photonics, leading to silicon-based photonic integrated circuits (PICs). Such circuits could be used, e.g., to establish very fast communication between circuit boards, between chips on a board, or even within single chips. There is a strong need for such fast communication links because the rapid progress of microprocessors may soon be severely limited by the transmission bandwidth capabilities of electronic connections made, e.g., of copper. Optical data transmission allows much higher data rates and would at the same time eliminate problems resulting from electromagnetic interference. The technology may also be useful for other areas of optical communications, such as fiber to the home (FTTH or generally FTTx).

Microphotonics is a related technology involving manipulation of light on a microscopic scale. It can be viewed upon as an equivalent to microelectronics, the electrical signal being replaced by an optical one. The analogy may become clearer when we consider the propagation of the signal. An electrical signal resides in the region of high electrical conductivity, whereas an optical signal propagates along the region of a high refractive index. The equivalent to an electrical wire in microphotonics is an optical waveguide, the refractive index of which is higher than that of the surrounding material.

Similarly, PICs correspond to electrical integrated circuits. The basic functions in PICs are the generation, guiding, splitting, multiplexing, amplification, switching, and detection of the light signal. It is possible to fabricate hybrid photonic devices, where the photonic functions are provided by structures made of III–V semiconductors (with a direct bandgap and electrooptic properties), such as, e.g., indium phosphide, and these are placed on a silicon chip containing the bulk of electronic components. There are some techniques based on epitaxial regrowth procedures or applying a sophisticated bonding process to combine a silicon chip containing waveguides with an indium phosphide-based laser chip providing the efficient coupling of the laser output light into other silicon photonic devices [59]. For that reason, hybrid devices tend to be expensive and are strongly limited in complexity. Still, all-silicon solutions, arising from the “siliconization of photonics,” would probably be more suitable for widespread applications.

7.3.1 Silicon-Photonic Circuits

Waveguides, splitters, couplers, mode transformers, tapers, and arrayed waveguide gratings (AWGs) belong to the basic building blocks of PICs. Optical splitters and couplers are used to split or couple light between different waveguides, mode transformers and tapers are used to couple the light from/to input/output fiber or between planar waveguides with different cross-sections, whereas AWGs are used for spatial combining or separation of different wavelengths. All these devices are constructed from combinations of various waveguide structures that create the basic elements of photonic devices.

7.3.2 Planar Silicon Waveguides

In optical applications, silicon is known in its oxidized form, silicon dioxide, as the basic material of the optical fiber. It offers a combination of a low material cost and relatively simple processing, and a useful temperature range makes it currently the best compromise among the various competing materials. Intense development work has resulted in the maturity and cost-efficiency of silicon-based fabrication technology. In silicon photonics devices, light is confined to the silicon material by a top and bottom cladding of silicon dioxide.

There are several waveguide structures that can be used to realize a waveguide on silicon, as shown in Fig. 7.29. The simplest is the slab waveguide (Fig. 7.29a), which has a uniform high-index core layer on a low-index cladding layer. When silicon is used as a waveguide core and is surrounded, for example by a SiO_2 cladding, a large index step is obtained. In such waveguides, light is highly confined in the core, which can have cross-sections as small as few hundreds of nanometers and the bending radius can be reduced to a few micrometers. The slab waveguide offers only vertical confinement, and cannot principally confine light horizontally. From the waveguide types offering full confinement, a channel waveguide (Fig. 7.29b) can be formed from the slab structure by photolithography and wet or dry etching techniques. After etching of the waveguide structure, a top cladding layer is typically deposited to provide a uniform low-index surrounding for the core. A variation of the strip waveguide is a ridge waveguide (Fig. 7.29c) in which the high-index core layer is not fully etched. However, the difference between the effective indices of the partially etched slab and the ridge is sufficient to confine light within the ridge section.

As there are several different waveguide structures available, there are also many materials that can be used to build a waveguide on silicon. These include, e.g., silicon dioxide, silicon oxynitride, polymers, germanium, structuring III–V semiconductors, and silicon itself. From the different material systems available, siliconon-on-insulator (SOI) is becoming an important platform for realizing PICs and for integrating them monolithically with control electronics. SOI technology takes advantage of commercially available SOI wafers that have a single-crystal Si layer (SOI layer) on top of a buried oxide (BOX) layer made of SiO_2. This structure readily acts as a slab waveguide. From this, the ridge waveguides fabrication is

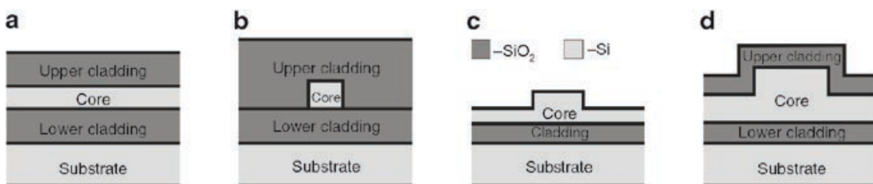

Fig. 7.29 Different waveguide structures: (**a**) slab waveguide, (**b**) channel waveguide, (**c**) ridge waveguide, and (**d**) ridge waveguide in SOI

straightforward as shown in Fig. 7.29d. Because of the ultra-high refractive index contrast between Si and SiO_2, SOI technology allows large-scale integration of optical circuits. Ultra-compact planar waveguide devices can thus be made in Si, and the transparency range includes the 1.3 and 1.55 μm telecommunication windows.

There are a number of techniques that can be used to grow the core and cladding materials for a waveguide on a silicon wafer. In principle, any of the deposition techniques known in microfabrication can be applied. These include thermal oxidation, sputtering, chemical vapor deposition, flame hydrolysis deposition, ion-assisted deposition, spin–coating, sol–gel technique, etc. [60]. The given application and chosen material system determine the requirements for the deposited thin film. However, there are some common requirements that the deposition technique must fulfill. First, the thin film should enable low optical losses. This means that the surface roughness should be low, and the material should have a negligible amount of impurities that can absorb light in the operating wavelength. For example, a high hydrogen content in a glass film grown with plasma enhanced chemical vapor deposition results in strong absorption at telecommunication wavelengths [61]. It is important to be able to control the film thickness accurately since the waveguide thickness is one of the main design parameters.

7.3.3 Moore's Law for Photonics and Beyond

The current state of photonic technology is such that a variety of different materials platforms are needed for different device functionalities. Thus, not only active devices such as lasers and modulators are needed, but also detectors, filters, multiplexers, wavelength converters, optical switches, and isolators. To do all this, we need to put photonics on the path of its own Moore's Law, when we could put photonics and electronics on a single chip [62].

This can be achieved by making the devices smaller, more efficient with less power consumption. Unlike electronics, where there is a single building block in the form of a complementary metal-oxide semiconductor (CMOS) transistor, photonics needs multiple functionalities. A most exciting prospect is that as the CMOS foundries decrease the feature size from 65 to 45 nm and, ultimately, 10 nm, the photonic devices can ride this progress and continue to become smaller, faster, and less power hungry. Once high performance photonic circuits can be created in a CMOS-compatible manner, they can coexist on the same of chip of silicon with electronic circuits [63].

Extending this materials capability to photonics and also merging the two primary device types, photonics and electronics, into one integrated dual functional device brings the benefits of large economy and wide applications, far beyond a simple combination of separate devices. With research growing in numerous industrial laboratories, one expects 100 Gbps devices for optical communication and novel devices for sensors and other application to be soon commercially available [62].

Acknowledgments The authors are grateful to Kouchi Zhang for stimulating and continuous encouragement of this work. **This chapter** is a review of the design and development of selected optoelectronics devices, and we are indebted to all of the researchers who have been contributing to this field. Only a few of these researchers are cited here, so we also thank those whose work has not been referenced. The authors are grateful to colleagues who have worked with them in this research since the early 1990s at the Microelectronics Department of the Slovak University of Technology in Bratislava in close collaboration with Slovak Academy of Science in Bratislava, University of Leipzig in Germany and City University of Hong Kong-COSDAF. The assistance of J. Breza and PhD students L. Peternai, J. Waclawek, and D. Hasko is greatly appreciated also.

This work was done in Center of Excellence CENAMOST (Slovak Research and Development Agency Contract. No. VVCE-0049–07) where support of European Commission projects, CP 93, No. 12 283, "DEMACOMINT" and IST-2001–32793-VGF GaP-LEDs as well as projects of the Slovak Research and Development Agency under the contracts APVV-20–055405 and APVV-0290–06 are gratefully acknowledged.

References

1. Suhir, E.: Microelectronics and photonics – the future. Microelectronics Journal **31,** 839–851 (2000)
2. Hecht, G.: Long-haul DWDM systems go to the distance. Laser Focus World, October, 125–132 (2000)
3. Mills, A.: Strategies in Light 2006: record LED sales but price erosion. III-V Review **29** (3), 35–39 (2006)
4. Türk, V., Bimberg, D.: Nanotechnology in optoelectronics - trends and prospects. Mstnews 3, 17–19 (1999)
5. Diff. authors: Things to watch in 2001, "High Brightness LEDs for Lightning", "Convergence of Optics and Electronics", "Explosive Market Growth for VCSELs", "Indium Phosphide Planar integrated Optics Comes of Age". Compound Semiconductor **7,** 45–84 (2001)
6. Nakamura, S.: III-V Nitride based light emitting devices. Solid State Communications **102 (2–3),** 237–242 (1997)
7. Forrest, S.R.: The road to high efficiency organic light emitting devices. Organic Electronics **4,** 45–4 (2003)
8. Kasap, S.O.: Optoelectronics and photonics, principles and practices. Prentice-Hall, Upper Saddle River, New Jersey (2001)
9. Suematsu, Y., Adams, A.R.: Semiconductor lasers and photonic integrated circuits. Chapman & Hall, London (1994)
10. Herman, M.A., Sitter, H.: Molecular beam epitaxy; Fundamentals and current status. Springer-Verlag, Berlin (1989)
11. Moon, R.L.: MOVPE: is there any other technology for optoelectronics? Journal of Crystal Growth **170,** 1–10 (1997)
12. Davies, J.H.: The physics of low-dimensional semiconductors: an introduction. Cambridge University Press, Cambridge, UK (1998)
13. Cingolani, R.: Semiconductor superlattices and interfaces. In: Proceedings of the International School of Physics "Enrico Fermi", Course CXVII, North-Holland (1993)
14. Kalt, H.: Optical properties of III-V semiconductors, Springer-Verlag, Berlin (1996)
15. Sullivan, S.C.: The anatomy of a quantum dot. Photonics Spectra 63 (2007)
16. Bergh, A.A., Dean, P.J.: Light-emitting diodes. Oxford University Press, Ely House, London (1976)
17. Wilkson, J., Hawkes, J.: Optoelectronics an introduction. Prentice Hall, London (1998)
18. Shaw, M.J., Seidler, P.F.: Organic electronics: introduction. IBM Journal of Research and Development **45(1),** 3–9 (2001)
19. Sheats, J.R., Antoniadis, H., Heuschen, M., Leonard, W., Miller, J., Moon, R., Roitman, D., Stocking, A.: Organic electroluminiscent devices. Science **273,** 913 (1996)

20. Dodapalabur, A., Torsi, L., Katz, H.E.: Organic transistors: two-dimensional transport and improved electrical characteristics. Science **268,** 270 (1996)
21. Kováč, J., Peternai L., Lengyel, O.: Advanced light emitting diodes structures for optoelectronic applications. Thin Solid Films **433,** 22–26 (2003)
22. Kováč, J., Wong, T.C., Fung, M.K., Liu, M.W., Kremnican, V., Bello, I., Lee, S.T.: Transient electroluminescence of single and multilayer organic light emitting devices. Materials Science and Engineering **B85,** 172–176 (2001)
23. Gardner, N.F., Chui, H.C., Chen, E.I., Kramers, M.R., Huang, J.-W., Kish, F.A., Stockman, S.A., Kocot, C.P., Tan, T.S., Moll, N.: 1Δ4§ efficiency improvement in transparent- substrate (AlGa)InP light -emitting diodes with thin active regions. Applied Physics Letters **74 (15),** 2230–2232 (1999)
24. Wallart, X., Deresmes, D., Mollot, F.: Growth of strained $Ga_{1-x}In_xP$ layers on GaP (100) by gas source molecular beam epitaxy: similarities and differences with the growth of strained arsenides. Journal of Grystal Growth 227–228, 255–259 (2001)
25. Peternai, L., Kováč, J., Jakabovič, J., Gottschalch V.: Numerical simulation and analysis of GaP/GaNP/GaP double heterostructure light emitting diode. In: WOCSDICE 2004 Proceedings, Smolenice Castle, Slovak Republic, 101–102 (2004)
26. Hasenöhrl, S., Novák, J., Vávra, I., Šatka, A.: Material properties of graded composition In_xGa1-xP buffer layers grown on GaP by OMVPE. Journal of Crystal Growth **272,** 633–641 (2004)
27. Novák, J, Hasenöhrl, S., Kúdela, R., Kučera, M.: Growth and characterisation of $In_xGa_{1-x}P$ layers with composition close to crossover from direct to indirect band gap. Journal of Crystal Growth 275, e1287–e1292 (2005)
28. Kováč, J., Peternai, L., Jakabovič, J., Šatka, A., Hasenöhrl, S., Novák, J., Gottschalch, V., Rheinläender, B.: New development of LED structures directly grown on GaP substrate. In: Proceedings "Electroluminiscence 2004", Toronto, Canada (2004)
29. Vincze, A., Šatka, A., Peternai, L., Ková , J., Hasenöhrl, S., Veselý, M.: SIMS and SEM analysis of $In_{1-x-y}Al_xGa_yP$ LED structure grown on $In_xGa_{1-x}P$ graded buffer. Applied Surface Science **252,** 7279–7282 (2006)
30. Mills, A.: High-brightness LEDs lightning up the future. III-Vs Review **14 (2),** 32–37 (2001)
31. Streubel, K., Linder, N., Wirth, R., Jaeger, A.: High brightness AlGaInP light-emitting diodes. IEE Journal of Selected Topics in Quantum Electronics **8 (2),** 321–331 (2002)
32. Kramers, M.R., Ochai-Holcomb, M., Hofler, G.E., Carter-Coman, C., Chen, E.I., Tan, I.H., Grillot, P., Gardner, N.F., Chui, H.C., Huang, J.W., Stockman, S.A., Kish, F.A., Tan, T.S., Kocot, C.P., Hueschen, M., Posselt, J., Loh, B., Sasser, G., Collins, D.: High-power truncatedinverted-pyramid (Al_xGa_{1-x})0:5In0:5P)/GaP light-emitting diodes exhibiting >50% external quantum efficiency. Applied Physics Letters **75 (16),** 2365–2367 (1999)
33. Cook, M.: Excitonic prospects for UV. III-V Review **29 (5),** 22–26 (2006)
34. Akasaki, I.: Nitride semiconductors-impact on the future world. Journal of Crystal Growth 237–239, 905–911 (2002)
35. Whitaker, T.: Innovations push white LEDs towards new applications. Compound Semiconductor **75** (2003)
36. Tang, C.W., Van Slyke, S.A.: Organic Electroluminescent Diodes. Applied Physics Letters **51**, 913 (1988)
37. Burroughes, J.H., Bradley, D.D.C., Brown, A.R., Marks, R.N., Mackay, K., Friend, R.H., Burns, P.L., Holmes, A.B.: Light-emitting diodes based on conjugated polymers. Nature **347,** 539 (1990)
38. Rentberger, S.: Doped OLEDs overcome limitations of traditional devices. Laser Focus World May, 79–84 (2007)
39. Bergh, A.: Commercial applications of optoelectronics. Photonics Spectra February, 54–61
40. Segler, D.J.: LEDs in high-definition television. Photonics Spectra, October, 62–65 (2007)
41. Ünlü, M.S., Strite, S.: Resonant cavity enhanced photonic devices. Journal of Applied Physics **78 (2),** 607–639 (1995)
42. Kishino, K., Ünlü, M. S., Chyi, J.-I., Reed, J., Arsenault, L., Morkoc, H.: Resonant cavity enhanced (RCE) photodetectors. IEEE Journal of Quantum Electron **27 (8),** 2025–2034 (1991)

43. Borgulová, J., Uherek, F., Kováč, J., Šatka, A.: Design of Multilayer Optoelectronic Devices. IEEE, SPIE Proc. Ser., 3820 (0277–786X/99), 239–247 (1999)
44. Waclawek, J.: Resonant cavity enhanced photodetectors. PhD thesis, Slovak University of Technology, Faculty of Electrical Engineering and Information Technology, Bratislava, Slovakia (1997)
45. Lai, K., Campbell, J.C.: Design of a tunable GaAs/AlGaAs multiple-quantum-well resonant-cavity photodetector. IEEE Journal of Quantum Electron **30 (1),** 108–114 (1994)
46. Waclawek, J., Kováč, J., Rheinländer, B., Gottschalch, V., Škriniarová, J.: Electrically tunable GaAs/AlGaAs MQW RCE Photodetector. Electronics Letters **33 (1),** 71–72 (1997)
47. Haško, D.: Lavínová fotodióda s oddelenou absorpčnou, nábojovou, a násobiacou vrstvou na báze InGaAs/InP (in Slovak language), PhD thesis, Slovak University of Technology, Faculty of Electrical Engineering and Information Technology, Bratislava, Slovakia (2005)
48. Haško, D., Kováč, J., Uherek, F., Škriniarová, J., Jakabovič, J., Peternai, L.: Avalanche photodiode with sectional InGaAsP/InP charge layer. Journal of Electrical Engineering **57 (6),** 369–372 (2006)
49. Harris, J.S. Jr: GaInNAs long-wavelength lasers: progress and challenges. Semiconductor Science and Technology **17,** 880–891 (2002)
50. Brennan, K.F., Haralson, J., Parks, J.W. jr., Salem, A.: Review of reliability issues of metal-semiconductor-metal and avalanche photodiode photonic detectors. Microelectronics Reliability **39 (12),** 1873–1883 (1999)
51. Budianu, E., Purica, M., Rusu, E.: Heterostructures on InP substrate for high-speed detection devices over a large spectral range (0:8–1:6mm). Microelectronics Engineering 51–52 (5), 393–400 (2000)
52. Saleh, M.A., Hayat, M.M., Kwon, O-H., Holmes, A.L., Campbell, J.C., Saleh, B.E.A., Teich, M.C.: Breakdown voltage in thin III-V avalanche photodiodes. Applied Physics Letters **79 (24),** 4037–4039 (2001)
53. Cho, S.R., Yang, S.K., Ma, J.S., Lee, S.D., Yu, J.S., Choo, A.G., Kim, T.I., Burm, J.: Suppression of avalanche multiplication at the periphery of diffused junction by floating guard rings in a planar InGaAs-InP avalanche photodiode. IEEE Photonics Technology Letters **12,** 534–536 (2000)
54. Watanabe, I., Nakata, T., Tsuji, M., Makita, K., Torikai, T., Taguchi, K.: High-speed, highreliability planar-structure superlattice avalanche photodiodes for 10-Gb/s optical receivers. Journal of Lightwave Technology **18,** 2200–2207 (2000)
55. Hecht, J.: Development of silicon photonics focuses on high speed optical interconnects. Laser Focus World, April, 86–89 (2007)
56. Boyraz, O., Jalali, B.: Demonstration of a silicon Raman laser. Optics Express **12 (21),** 5269 (2004)
57. Rong, H., et al.: Low-threshold continuous-wave Raman silicon laser. Nature Photonics **1 (4),** 232 (2007)
58. Greene, K.: Intel speeds up silicon photonics. In: Technology Review, Infotech, January 22 (2007)
59. Jones, R., Cohen, O., Paniccia, M., Fang, A.W., Bowers, J.: The first electrically pumped, hybrid silicon laser overcomes one of the major hurdles to photonic chips. Photonics Spectra, January, 55–63 (2007)
60. Cheben, P.: Wavelength dispersive planar waveguide devices: Echelle gratings and arrayed waveguide gratings. In: Optical waveguides: from theory to applied technologies, M. L. Calvo and V. Laksminarayanan, Eds., Chapter 5, Taylor & Francis, London, 174–217 (2007)
61. Osinsky, A.V., Bellman, R.A., Akwani, I.A., Sachenik, P.A., Logunov, S.L., McCamy, J.W.: Optical loss mechanisms in GeSiON planar waveguides. Applied Physics Letters 81 (11), 2002–2004 (2002)
62. Melle, S.: Network capacity growth demands new solutions. Laser Focus World, October, 113–115 (2006)
63. Salib, M., at al.: Silicon photonics. Intel Technology Journal 8 (2), 143–160 (2004)